Advanced Steel Construction – Vol. 21 No. 1 (2025) 42–53
DOI:10.18057/IJASC.2025.21.1.4

SECOND-ORDER INELASTIC ANALYSIS OF STEEL FRAME STRUCTURES USING IMPROVED FIBER PLASTIC HINGE METHOD

Fan Xu [1, 2], Yi-Qun Tang [1, 2, *], Xiao-Meng Ding [1, 2], De-Hong Huang [3, 4] and Yao-Peng Liu [3, 4]

[1] *School of Civil Engineering, Southeast University, Nanjing, China;*
[2] *Jiangsu Key Laboratory of Mechanical Analysis for Infrastructure and Advanced Equipment, Nanjing, China*
[3] *School of Civil Engineering and Transportation, South China University of Technology, Guangzhou 510641, China;*
[4] *State Key Laboratory of Subtropical Building and Urban Science, South China University of Technology, Guangzhou 510641, China*
* *(Corresponding author: E-mail: yi-qun.tang@seu.edu.cn)*

A B S T R A C T

In the realm of inelastic analysis for steel structures, the plastic hinge method is recognized for its computational efficiency but is often criticized for its lower accuracy than the plastic zone method. The present study aims to improve the accuracy of the plastic hinge method by discretizing the cross-section of the plastic hinges located at the element ends. Besides, the proposed fiber plastic hinge method is more efficient than the plastic zone method where each cross-section at the integration points of the element should be discretized. This study utilizes the improved fiber plastic hinge method to compute the initial and full yield surfaces of the cross-section, determine the section spring stiffness, and integrate this method into the second-order inelastic analysis of steel frame structures. Several classic benchmark problems are solved by the present method and the obtained results are compared with results generated by the plastic zone method as implemented in finite element software. The comparison reveals that the proposed fiber plastic hinge method matches the plastic zone method in terms of high accuracy for predicting the inelastic behavior of steel structures, with the added advantage of greater efficiency.

A R T I C L E   H I S T O R Y

Received: 10 September 2024
Revised: 10 September 2024
Accepted: 9 October 2024

K E Y W O R D S

Steel structures;
Second-order inelastic analysis;
Fiber plastic hinge;
Beam-column element;
Transverse shear deformation

Copyright © 2025 by The Hong Kong Institute of Steel Construction. All rights reserved.

1. Introduction

Over the past several decades, technological advancements have significantly accelerated the evolution of the second-order analysis method for steel frame structures. The second-order analysis can fully account for the geometric nonlinearities of the P-Δ and P-δ effects. Thus, it eliminates the need to consider the effective length of each component during the stability design process, and the classification of the frame in the analysis process is not required. In light of this, it has been fully integrated into the steel structure design codes of numerous countries [1]. To predict more accurately the actual response of the steel structure, the influence of material nonlinearity should be taken into account in the analysis [2]. However, considering both geometric and material nonlinearities in analysis consumes a considerable amount of time. Therefore, improving both the accuracy and efficiency of second-order inelastic analysis for steel frame structures is a pivotal research topic.

The second-order plastic hinge analysis method based on the concept of one element per member has been verified as efficient and suitable for practical engineering design [5,6]. It enables the simulation of steel structures with fewer nodes and elements, thereby markedly reducing computational costs [7-9]. To ensure the accuracy of the local second-order effect in the displacement-based beam-column element, high-order interpolation should be adopted in the derivation of element formulations. For instance, Lu et al. [10] utilized a fourth-order polynomial function to simulate the vertical displacement of the beam-column element, deriving a fourth-order element and conducting the nonlinear analysis of steel structures. Chan et al. [11][12] introduced the pointwise equilibrating polynomial (PEP) element, which adopts a fifth-order polynomial function to model the vertical displacement of the beam-column element, achieving significantly higher computational accuracy than other elements. Based on the PEP element, Tang et al. [13] proposed a new second-order beam-column element based on Timoshenko beam theory. Both transverse shear deformation and local second-order effect are taken into account simultaneously in the element formulations, enabling accurate results to be obtained using only one element per member in structural analysis. Doan-Ngoc et al. [14] further improved the accuracy of the calculation by using an approximate seventh-order polynomial function to simulate the vertical displacement of the element.

The plastic zone method and the plastic hinge method are the mainstream approaches for the inelastic analysis of steel frame structures. The former approach discretizes the cross-section and length of the element, so it requires significant computational resources and can provide nearly exact solutions. The latter approach considers the inelastic behavior of the steel member only at the element ends and the discretization of cross-section is commonly not required in the analysis. Thus, the derived elastic second-order beam-column elements can be integrated with the plastic hinge method to realize the second-order inelastic analysis of steel frame structures with relatively low effort. However, the accuracy of the plastic hinge method is not as good as the plastic zone method. To enhance it, many researchers have contributed great efforts in the last three decades.

In early research about the second-order plastic hinge analysis of steel frame structures, Kassimal et al. [15] proposed a simple plastic hinge model and integrated it with the stability functions which are closed-form solutions of the second-order beam-column element based on Euler-Bernoulli beam theory. In this model, the hinges at element ends are assumed to be ideally elastoplastic and overlook the gradual yielding process of the hinge cross-section, resulting in reduced precision in modeling the elastoplastic behavior of the element. To solve this issue, Liew et al. [16] introduced a refined plastic hinge method that considers a gradual reduction in the inelastic stiffness of the element. Nguyen et al. [17] considered the gradual yield of plastic hinges by introducing a stiffness degradation formula for springs at both ends of beam-column elements. Zhou et al. [18] proposed an improved refined plastic hinge model using an approximate sixth-order polynomial function to simulate transverse displacements in beam-column elements, incorporating second-order effects between axial loads and bending moments into the element formulation. Liu et al. [19][20] proposed a new type of beam-column element, in which a plastic hinge can be formed at any position on the element. For nonlinear materials with obvious hardening effects, such as stainless steel, Fieber et al.[21][22], Gardner et al.[23], Walport et al.[24], and Quan et al. [25] proposed a new approach for second-order inelastic analysis of steel frame structures.

Although many researchers have endeavored to improve the accuracy of the plastic hinge model, the differences in precision between the plastic hinge model and the plastic zone model are still apparent. Thus, this paper aims to further improve the precision of the plastic hinge model in the second-order inelastic analysis of steel frame structures. The present study proposes modifications to the classic end-spring-type plastic hinge model through the incorporation of the fiber plastic hinge concept. The classic model comprises a second-order beam-column element and two zero-length spring elements positioned at both ends, assuming that the beam-column element is in an elastic state throughout and elastoplastic behavior is only confined to the spring elements [3][4]. The accuracy of this model depends primarily on determining the initial and full yield surfaces of the cross-section, as well as the spring stiffness, which is typically empirical and approximate. Thus, the present study discretizes the sections of the spring elements and computes more accurate initial and full yield surfaces of the cross-section, as well as the moment-curvature relationship. Then, the length of the plastic hinge and the spring stiffness are determined according to numerical tests. Furthermore, to ensure the accuracy of the structural analysis using one element per member, this study adopts a second-order beam-column element based on the Timoshenko beam theory [13]. The element takes into account both local second-order effects and transverse shear deformation. In addition, the present study integrates an advanced incremental-iterative force recovery method [26]. Finally, several benchmark problems are solved by the present study, and the results are compared with those from previous literature and the plastic zone method in ANSYS. The comparison verifies the accuracy, efficiency, and robustness of the proposed methodology and computational program for the second-order inelastic analysis of steel frame structures using only one element per member.

2. Element model and assumptions

Assumptions for the planar element model in this study are given as follows: 1. The applied loads are nodal and conservative; 2. The cross-section of the member is doubly symmetric and remains planar after deformation, neglecting warping and torsion; 3. The element exhibits small-strain and large-displacement characteristics; 4. The transverse shear deformation of the members is considered based on Timoshenko beam theory, while the local second-order effects (bowing effects) in the element are permitted; 5. The interior beam-column element is prismatic and elastic throughout the inelastic analysis, situated between the two spring elements; 6. The elastoplastic behavior of the element is confined to its ends where plastic hinges are simulated using zero-length springs; 7. The material is assumed to be elastic-perfectly plastic, ignoring strain-hardening effects.

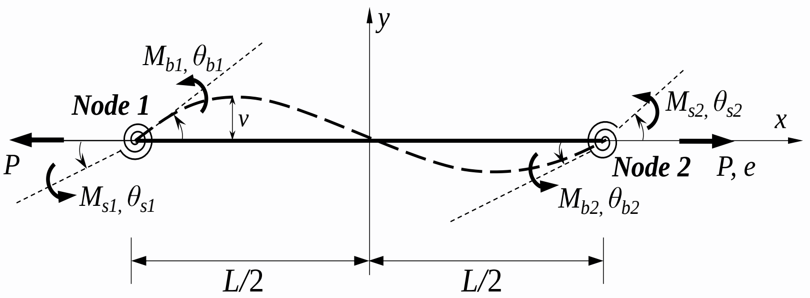

Fig. 1. Beam-column element model with plastic hinges

Fig. 1 depicts a beam-column element with two spring elements at both ends, where L represents the length of the beam-column element; E and I denote Young's modulus and moment of inertia, respectively. M_{si} (i=1,2) are the bending moments acting on the external nodes i, with θ_{si} (i=1,2) being the corresponding rotations. M_{bi} (i=1,2) signifies the bending moments acting on internal node i, located at the interface between the spring elements and the beam-column element, with θ_{bi} (i=1,2) as their respective rotations. P and e represent the axial force and axial displacement of the element, respectively. $v(x)$ denotes the transverse displacement function of the element.

3. Improved fiber plastic hinge method

In the traditional end-spring-type plastic hinge model, the full yield surface of the cross-section and the spring stiffness are determined commonly using a simplified and empirical method, therefore it is difficult to obtain accurate results as good as those by the plastic zone model. To fill this gap, the present study utilizes the fiber hinge concept to improve the accuracy of the end-spring-type plastic hinge model. This section presents how to utilize the improved fiber plastic hinge method for calculating the initial and full yield surfaces, the moment-curvature curve of the cross-section, as well as the stiffness of the fiber section spring element.

3.1. Discretion of wide flange section

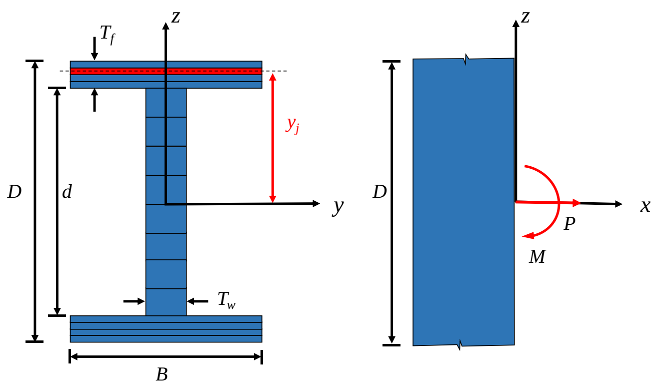

Fig. 2. Discretization of cross-section

Fig. 2 depicts the discretization of the wide flange section under the axial force P and the major-axis bending M. Assume that the stress at the j-th fiber σ_j is uniform, so the axial force P and the major-axis bending M can be given by,

$$P = \sum_{j=1}^{N} \sigma_j A_j \tag{1}$$

$$M = \sum_{j=1}^{N} \sigma_j A_j y_j \tag{2}$$

in which, A_j represents the area of the j-th fiber; y_j denotes the distance from the centroid of the j-th fiber to the center of the wide flange section. Besides, this paper denotes the width and height of the j-th fiber as b_j and Δh_j, respectively; N is the total number of fibers in the section.

3.2. Initial and full yield surfaces of fiber section

When the wide flange section is subjected to a combined action of axial force and bending moment, for a given axial force P, the ultimate elastic moment capacity of the section can be easily given as follows

$$M_{er} = (\sigma_y - \frac{P}{A})\frac{I}{y_{j\max}} \tag{3}$$

where A is the total section area, σ_y represents the yield stress and I is the moment of inertia of the cross-section about the major axis z; y_{jmax} denotes the distance from the centroid of a layer of fibers farthest from the neutral axis.

When the wide flange section reaches the ultimate limit state of bearing capacity, stresses at all fibers are equal to the yield stress, as shown in Fig. 3. Furthermore, the offset of the neutral axis from the center of the cross-section β should be considered in the determination of the ultimate plastic moment capacity of the discrete wide flange section.

Residual stresses are not considered herein, so the offset of the neutral axis from the center of the cross-section β can be calculated in the following,

$$p = \frac{P}{P_y} \tag{4}$$

$$\beta = \frac{p \cdot A}{2T_w} \qquad for \quad p < \frac{A_W}{A} \tag{5}$$

$$\beta = \frac{p \cdot A - A_F - A_W}{2B} + \frac{D}{4} + \frac{d}{4} \qquad for \quad p \geq \frac{A_W}{A} \; \&\& \; p \leq 1 \tag{6}$$

where P_y is the axial force capacity of the cross-section; A_w represents the area of the web, and A_F is the area of the flange.

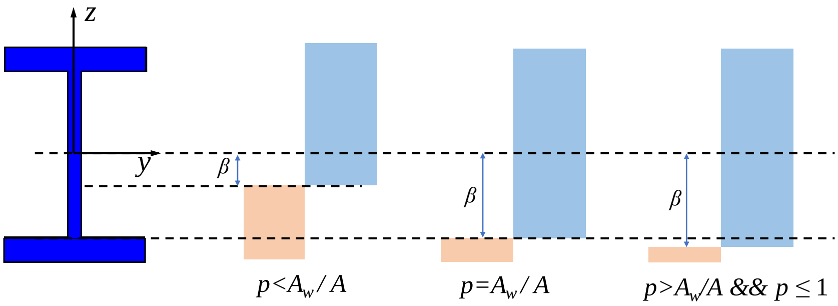

Fig. 3. Diagram of the complete yield stress under different axial forces

After the calculation of β, the ultimate plastic moment capacity M_{pr}, which the axial force may reduce, can be defined as the sum of three parts,

$$M_{pr} = M_{p1} + M_{p2} + M_{p3} \tag{7}$$

$$M_{p1} = -\sum b_j \cdot \Delta h_j \cdot y_j \cdot \sigma_y \qquad for\ y_j + \frac{\Delta h_j}{2} \le -\beta \tag{8}$$

$$M_{p2} = \sum b_j \cdot \Delta h_j \cdot y_j \cdot \sigma_y \qquad for\ y_j - \frac{\Delta h_j}{2} \ge -\beta \tag{9}$$

$$M_{p3} = \sum\left(\frac{\sigma_y b_j (y_j + \frac{\Delta h_j}{2} + \beta)(y_j + \frac{\Delta h_j}{2} - \beta)}{2} - \frac{\sigma_y b_j (-\beta - (y_j - \frac{\Delta h_j}{2}))(y_j - \frac{\Delta h_j}{2} - \beta)}{2}\right) \qquad for \quad y_j + \frac{\Delta h_j}{2} > -\beta \ \&\& \ y_j - \frac{\Delta h_j}{2} < -\beta \tag{10}$$

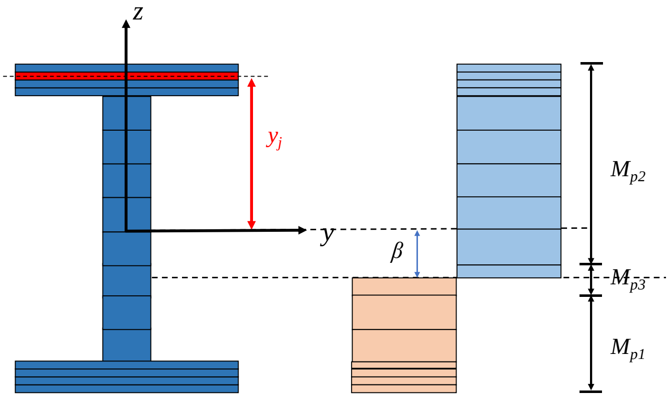

Fig. 4. The calculation of the ultimate moment capacity

Fig. 4 shows the definitions of the three parts contributing to the ultimate plastic moment capacity. When the j-th fiber is completely located below the neutral axis, its contribution to the cross-section's moment capacity is M_{p1} in Eq. (8). When the j-th fiber is completely located above the neutral axis, its contribution to the cross-section's moment capacity is M_{p2} given by Eq. (9). M_{p3} is calculated by artificially dividing the layer of fiber into two parts when the neutral axis of the cross-section intersects during the layer, resulting in Eq. (10). When P is equal to zero, M_{pr} is equal to the ultimate plastic moment capacity of the cross-section only under pure bending, M_p.

The ultimate elastic moment capacity M_{er} and the ultimate plastic moment capacity M_{pr} of the cross-section can be computed by Eq. (3) and Eqs. (7-10), respectively. The initial and full yield surfaces are depicted in Fig. 5 according to the calculation of M_{er} and M_{pr} for a given axial force P. Fig. 6 shows the cross-section's stress distributions during the gradual yielding process under a fixed axial force P, where the stress distributions of Points 1, 2, and 3 correspond to the points in Fig. 5. Note that the derivation of the initial yield surface and the full yield surface is calculated based on the wide flange section of W21×50.

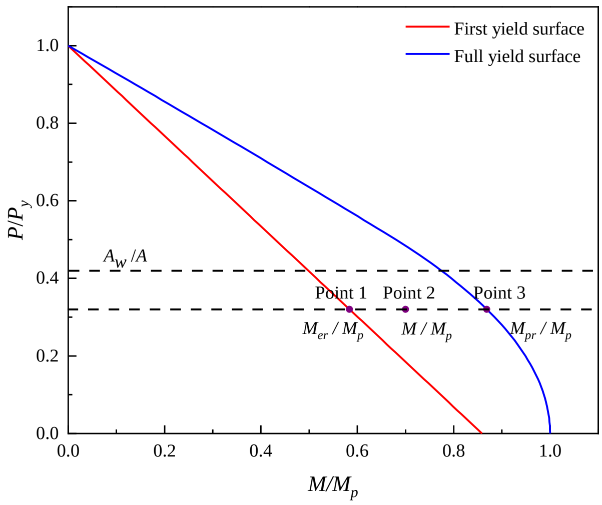

Fig. 5. First and full yield surfaces of section

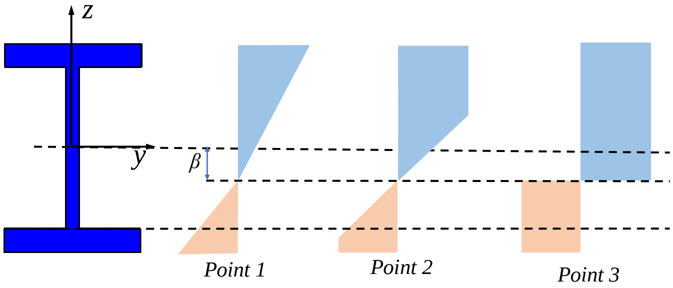

Fig. 6. Stress distribution

As shown in Fig. 5 and Fig. 6, the section is within the elastic range when the axial force and bending moment are within the initial yield surface. The section partially yields when the load coordinates between the initial and full yield surfaces. As the bending moment M increases, the extent of section yielding progressively intensifies, ultimately culminating in the full yield surface.

3.3. Moment-curvature curve for wide flange section

During an incremental-iterative load step of the end-spring-type plastic hinge analysis, the stiffness of the spring element is determined by the current forces applied to the spring element. Thus, this study employs the axial force and the bending moment applied to the fiber plastic hinge to calculate its curvature and the offset of the neutral axis.

According to the assumption of the elastic-perfectly plastic material model, the stress at the j-th layer of the cross-section is

$$\sigma_j = \begin{cases} E\varepsilon_j & for \quad \varepsilon_j < \sigma_y / E \\ \sigma_y & for \quad \varepsilon_j \geq \sigma_y / E \end{cases} \tag{11}$$

in which E is Young's modulus; ε_j is the strain at the j-th layer of the cross-section. It can be given as follows,

$$\varepsilon_j = \varepsilon_0 + \kappa(y_j + \beta) \tag{12}$$

where ε_0 is the strain due to the axial force P and it equals P/EA; κ and β are the curvature and the offset of the neutral axis of the cross-section, respectively.

The tangent modulus of the j-th layer of the cross-section can be easily given as follows,

$$E_{tj} = \begin{cases} E & for \quad \varepsilon_j < \sigma_y / E \\ 0 & for \quad \varepsilon_j \geq \sigma_y / E \end{cases} \tag{13}$$

To determine the curvature κ and the offset of the neutral axis β of the cross-section based on the known axial force F^n and the bending moment M^n at the current load step n, the *Newton-Raphson* iteration procedure should be constructed in the following,

$$\begin{bmatrix} \beta_{k+1} \\ \kappa_{k+1} \end{bmatrix} = \begin{bmatrix} \beta_k \\ \kappa_k \end{bmatrix} - \begin{bmatrix} \frac{\partial M_k}{\partial \beta} & \frac{\partial M_k}{\partial \kappa} \\ \frac{\partial P_k}{\partial \beta} & \frac{\partial P_k}{\partial \kappa} \end{bmatrix}^{-1} \begin{bmatrix} M^n - M_k \\ P^n - P_k \end{bmatrix} \tag{14}$$

$$\frac{\partial M_k}{\partial \beta} = E_{tj} \cdot \kappa \cdot b_j \cdot \Delta h_j \cdot y_j \tag{15}$$

$$\frac{\partial M_k}{\partial \kappa} = E_{tj} \cdot (y_j + \beta) \cdot b_j \cdot \Delta h_j \cdot y_j \tag{16}$$

$$\frac{\partial P_k}{\partial \beta} = E_{tj} \cdot \kappa \cdot b_j \cdot \Delta h_j \tag{17}$$

$$\frac{\partial P_k}{\partial \kappa} = E_{tj} \cdot (y_j + \beta) \cdot b_j \cdot \Delta h_j \tag{18}$$

in which the axial force P_k and the moment M_k are computed by substituting the curvature κ_k and the offset of the neutral axis β_k at the k-th iteration into Eqs. (12), (11), (1), and (2) in sequence.

The iteration procedure in Eq. (14) terminates when the following convergence criteria are satisfied,

$$\left| \frac{M^n - M_k}{M^n} \right| \leq Tolerance \tag{19}$$

$$\left| \frac{P^n - P_k}{P^n} \right| \leq Tolerance \tag{20}$$

in which *Tolerance* is set to 10^{-6} in the present study.

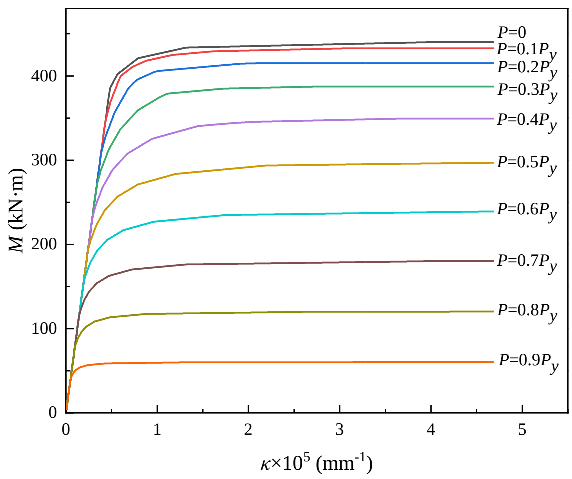

Fig. 7. Moment-curvature curves at different axial forces

Based on the algorithm presented before, Fig. 7 shows moment-curvature curves at different axial forces, taking the wide flange section of W21×50 for example.

3.4. Stiffness of fiber section spring element

In the end-spring-type plastic hinge model, the stiffness of the section spring element is infinite when it is elastic, which means that the difference in rotation between the spring element and the interior beam-column element is zero. The stiffness varies from infinity to zero as the moment transitions from initial yielding to full yielding. Thus, in the computational procedure, the spring stiffness is set to a large value, 10^{10} *EI/L*, instead of infinity when the spring element is elastic, while the spring stiffness is set to zero when the spring element is fully plastic. The key point of the end-spring-type plastic hinge model lies in the definition of the spring stiffness during partial yielding which controls the gradual yielding progress of the member. Therefore, this section introduces how to determine the spring stiffness during partial yielding based on the improved fiber plastic hinge method.

Fig. 8 presents the moment-curvature curve for the section of W21×50 under pure major-axis bending moment. Where M_{pr} is calculated by Eq. (7) and M_{er} is calculated by Eq. (3). It can be seen from Fig. 8 that the total curvature κ can be divided into two parts when the section partially yields, including the elastic curvature κ_e and the plastic curvature κ_p.

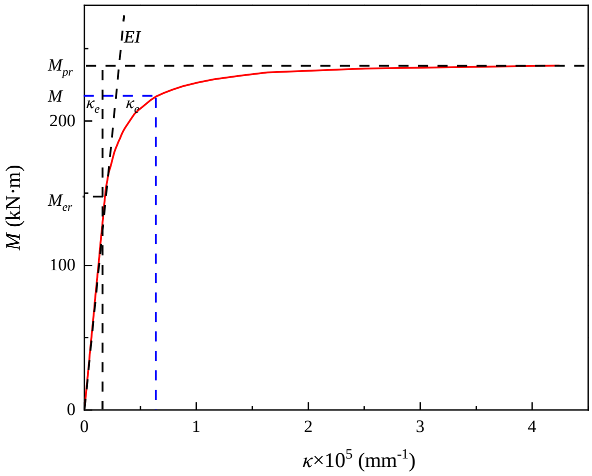

Fig. 8. Moment-curvature curve

Note that the difference in nodal rotation between the spring element and the interior beam-column element during the partial yielding state is due to the plastic deformation of the spring element. Thus, the spring stiffness during partial yielding is related to the relationship between moment and plastic curvature. Fig. 9 presents the moment-plastic curvature curve, from which the differential relationship between moment and plastic curvature can be derived as follows

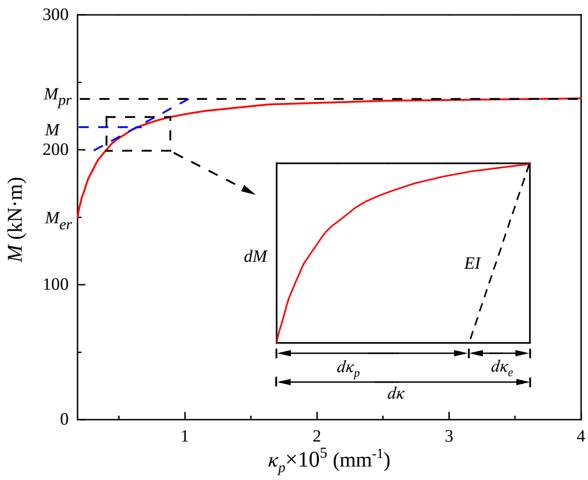

Fig. 9. Moment-plastic curvature curve

$$\frac{\mathrm{d}M}{\mathrm{d}\kappa_\mathrm{p}}=\frac{\dfrac{\mathrm{d}M}{\mathrm{d}\kappa}\dfrac{\mathrm{d}M}{\mathrm{d}\kappa_\mathrm{e}}}{\dfrac{\mathrm{d}M}{\mathrm{d}\kappa_\mathrm{e}}-\dfrac{\mathrm{d}M}{\mathrm{d}\kappa}} \tag{21}$$

$$\frac{\mathrm{d}M}{\mathrm{d}\kappa_\mathrm{e}}=EI_z \tag{22}$$

$$\frac{\mathrm{d}M}{\mathrm{d}\kappa}=-\sum Et_j\cdot\left(-y_j+\beta\right)\cdot b_j\cdot\Delta h_j\cdot y_j \tag{23}$$

In the end-spring-type plastic hinge model, the spring stiffness is defined as the relationship between moment and rotation. Thus, to transfer the differential relationship between moment and plastic curvature into the spring stiffness, a parameter named the length of the plastic hinge L_p is assumed, and the spring stiffness S_s can be given by,

$$S_\mathrm{s}=\frac{\mathrm{d}M}{\mathrm{d}\theta_\mathrm{p}}=\frac{1}{L_\mathrm{p}}\frac{\mathrm{d}M}{\mathrm{d}k_\mathrm{p}} \tag{24}$$

This study performed a large number of numerical tests of several wide flange sections under various loading combinations. The comparison between the present plastic hinge model and the plastic zone model shows that the length of the plastic hinge is mainly affected by the bending moments at member ends and the member's axial force level. The plastic hinge length L_p of the spring element during partial yielding is fitted according to the results from the simulation by the BEAM188 element in ANSYS in the following,

$$L_p = (0.02388e^{0.6789\xi} + 0.0003397e^{7.394\xi})\,(8.282e^{0.9745p} - 7.376e^{-7.109p})\,L \tag{25}$$

$$\xi = -\frac{\min\{|M_1|,|M_2|\}}{\max\{|M_1|,|M_2|\}} \qquad for\ \ M_1M_2 > 0 \tag{26}$$

$$\xi = \frac{\min\{|M_1|,|M_2|\}}{\max\{|M_1|,|M_2|\}} \qquad for\ \ M_1M_2 \le 0 \tag{27}$$

where M_1 is the bending moment at the member end associated with the current plastic hinge, M_2 is the bending moment at the other end of the member; and the abscissa ξ is the ratio of the two end moments. Fig. 10 shows the bending moment diagram of the member at different ratios of two end moments.

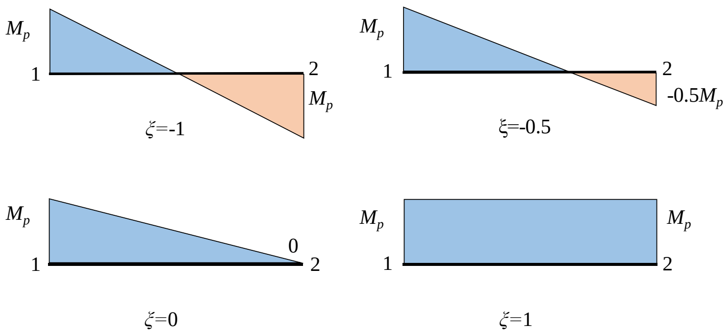

Fig. 10. Bending moment diagram of a member

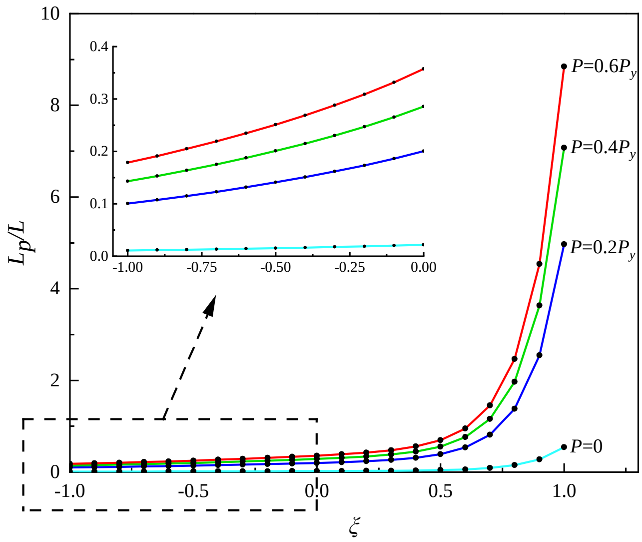

Fig. 11. Normalized L_p at different loadings

The length of plastic hinge L_p under different loadings is plotted in Fig. 11. It is observed that the length of the plastic hinge in a member tends to increase with the magnitude of the axial load and the ratio of the bending moments at the two ends of the member. However, the increase in plastic hinge length is less significant when the ratio of the end moments is negative, and it becomes more pronounced when this ratio exceeds 0.5.

4. Second-order inelastic analysis of steel frame structures

The improved fiber plastic hinge method is integrated into the second-order inelastic analysis of steel frame structures using one element per member. Additionally, this study employs a second-order beam-column element that accounts for both transverse shear deformation and bowing effects. It also utilizes a rigorous incremental-iterative recovery force method to further enhance the analysis's accuracy.

The integrated element model shown in Fig. 1 comprises an elastic second-order beam-column element and two spring elements. The two key factors in the nonlinear analysis are the tangent stiffness and the internal forces of the integrated element. Here the displacement and force vectors of the integrated element are denoted as $\boldsymbol{d}_s=\{\theta_{s1}, \theta_{s2}, e\}^{\mathrm{T}}$ and $\boldsymbol{f}_s=\{M_{s1}, M_{s2}, P\}^{\mathrm{T}}$, respectively.

4.1. Second-order beam-column element

The interior beam-column element adopted herein is proposed by Tang et al. [13]. It is derived from the Timoshenko beam theory, which incorporates both the bowing effect and the transverse shear deformation. As shown in Fig. 12, the element uses a fifth-order polynomial to assume transverse displacements, ensuring high accuracy using just one element per member in the analysis.

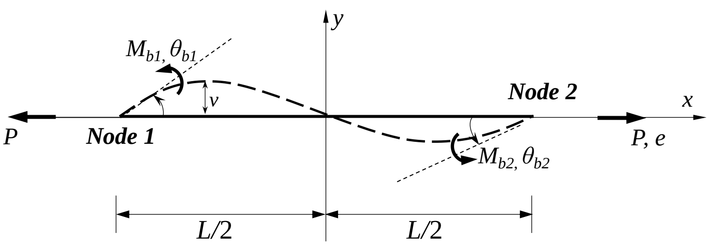

Fig. 12. Beam-column element

In the basic coordinate system, the presented beam-column element has three degrees of freedom, see Fig. 12. Its nodal displacement vector is $\boldsymbol{d}_b=\{\theta_{b1}, \theta_{b2}, e\}^{\mathrm{T}}$, while the corresponding nodal load vector is $\boldsymbol{f}_b=\{M_{b1}, M_{b2}, P\}^{\mathrm{T}}$. The secant relationships between the forces and the displacements of the element are given as follows:

$$M_{b1} = \frac{EI}{L}(S_1\theta_{b1} + S_2\theta_{b2}) \tag{28}$$

$$M_{b2} = \frac{EI}{L}(S_2\theta_{b1} + S_1\theta_{b2}) \tag{29}$$

$$P = EA(\frac{e}{L} + c_{\mathrm{b}}) \tag{30}$$

and

$$c_{\mathrm{b}} = b_1(\theta_{b1} + \theta_{b2})^2 + b_2(\theta_{b1} - \theta_{b2})^2 \tag{31}$$

where S_i (i=1, 2) and b_i (i=1, 2) represent the stability functions considering the bowing effect and bow functions in the beam-column element, respectively. c_b is the length correction factor due to the bowing effect. For the sake of simplification, these functions are not detailed in this paper and can be found in Reference [26].

4.2. Tangent stiffness of the integrated element

In the incremental-iterative process of nonlinear structural analysis, the tangent stiffness of the integrated element is crucial, significantly influencing the convergence rate of the analysis. It is assembled by the tangent stiffness matrices of the interior beam-column element and the two spring elements.

The tangent stiffness matrix of the beam-column element is derived by variational operations on Eqs. (28-30). The resulting matrix is presented as follows,

$$[\boldsymbol{k}_e] = \frac{\partial \boldsymbol{f}}{\partial \boldsymbol{d}^T} \tag{32}$$

$$[\boldsymbol{k}_e] = \frac{EI}{L}\begin{bmatrix} \frac{1}{L^2 H} & \frac{G_1}{LH} & \frac{G_2}{LH} \\ & c_1 + c_2 + \frac{G_1^2}{H} & c_1 - c_2 + \frac{G_1 G_2}{H} \\ \text{sym.} & & c_1 + c_2 + \frac{G_2^{\,2}}{H} \end{bmatrix} \tag{33}$$

where the parameters H, G_1, G_2, c_1 and c_2 in Eq. (33) can be found in Reference [13].

After the determination of the spring stiffness, the differential moment-rotation relationship of the spring element located at node i of the element model can be easily given as follows,

$$\begin{Bmatrix} dM_{si} \\ dM_{bi} \end{Bmatrix} = \begin{bmatrix} S_{si} & -S_{si} \\ -S_{si} & S_{si} \end{bmatrix}\begin{Bmatrix} d\theta_{si} \\ d\theta_{bi} \end{Bmatrix} \quad (i=1, 2) \tag{34}$$

The tangent stiffness matrix of the end spring calculated in Eq. (34) and the tangent stiffness matrix of the beam-column elements calculated in Eq. (33) are assembled to form the overall tangent stiffness matrix of the integrated element. Note that the assembled moments, M_{b1} and M_{b2}, acting on the inner degrees of freedom, θ_{b1} and θ_{b2}, are zeros. Thus, the inner degrees of freedom, θ_{b1} and θ_{b2}, can be condensed in the assembled tangent stiffness matrix, leading to a 3×3 tangent stiffness matrix of the integrated element. This process is a classical finite element procedure and will not be described in detail herein.

After the determination of the tangent stiffness of the integrated element in the basic coordinate system, it can be transferred into the global system through the co-rotational technique and assembled into the tangent stiffness matrix of the whole structure.

4.3. Incremental iterative force recovery method

In the incremental-iterative process of nonlinear structural analysis, the force recovery method is pivotal to the accuracy of the results. Consequently, this study adopts a rigorous incremental-iterative force recovery method, as proposed by Tang et al. [26], to ensure a high level of precision in the analysis. This force recovery method adopts the incremental secant relationship between forces and displacements for the second-order beam-column element, offering greater precision than traditional methods that rely on the incremental tangent relationship of the element.

After an iteration of nonlinear structural analysis, the incremental pure deformations of the integrated element $\Delta\boldsymbol{d}_s=\{\Delta\theta_{s1}, \Delta\theta_{s2}, \Delta e\}^{\mathrm{T}}$ can be extracted from the incremental global displacements of the structure based on the co-rotational technique. Then, the internal forces of the integrated element at the current load step n+1 can be computed according to the incremental pure deformations of the integrated element and the known quantities of the element at the last load step n.

For the interior beam-column element, the incremental secant relationship between forces and displacements for the second-order beam-column element are,

$$\Delta M_{b1} = \frac{EI}{L}\left(S_1^{n+1}\Delta\theta_{b1} + S_2^{n+1}\Delta\theta_{b2} + \Delta S_1\theta_{b1}^n + \Delta S_2\theta_{b2}^n\right) \tag{35}$$

$$\Delta M_{b2} = \frac{EI}{L}\left(S_2^{n+1}\Delta\theta_{b1} + S_1^{n+1}\Delta\theta_{b2} + \Delta S_2\theta_{b1}^n + \Delta S_1\theta_{b2}^n\right) \tag{36}$$

$$\Delta P = EA\left(\frac{\Delta e}{L} + \Delta c_b\right) \tag{37}$$

and

$$\Delta M_{bi} = M_{bi}^{n+1} - M_{bi}^n \quad (i=1, 2) \tag{38}$$

$$\Delta S_i = S_i^{n+1} - S_i^n \quad (i=1, 2) \tag{39}$$

$$\Delta c_b = c_b^{n+1} - c_b^n \tag{40}$$

For the spring element at node i of the integrated element, the differential moment-rotation relationship depicted in Equation (34) from the last load step n is utilized to approximate its incremental relationship during both the elastic and partial yielding states. It can be given as follows,

$$\Delta M_{si} = S_{si}^n\left(\Delta\theta_{si} - \Delta\theta_{bi}\right) \quad (i=1, 2) \tag{41}$$

$$\Delta M_{bi} = S_{si}^n\left(\Delta\theta_{bi} - \Delta\theta_{si}\right) \quad (i=1, 2) \tag{42}$$

Once the spring element is fully plastic, its applied moment will stay on the full yield surface in the subsequent analysis process, and the incremental moment is the difference in the plastic moment capacity ΔM_{pr} which will be reduced due to the increase of the axial load. Therefore, when the spring element reaches a fully plastic state, Equations (41) and (42) should be superseded by the following equations

$$\Delta M_{si} = \Delta M_{pr,i} \quad (i=1, 2) \tag{43}$$

$$\Delta M_{bi} = \Delta M_{pr,i} \quad (i=1, 2) \tag{44}$$

It is noted that the bending moment M_{bi} at the inner degrees of freedom of the integrated element, θ_{b1} and θ_{b2}, must be zero (M_{bi}=0), implying that the increment of the bending moment ΔM_{bi} is also zero. Consequently, the following relationship can be established.

$$\frac{EI}{L}\left(S_1^{n+1}\Delta\theta_{b1} + S_2^{n+1}\Delta\theta_{b2} + \Delta S_1\theta_{b1}^n + \Delta S_2\theta_{b2}^n\right) + \Delta M_{b1} = 0 \tag{45}$$

$$\frac{EI}{L}\left(S_2^{n+1}\Delta\theta_{b1} + S_1^{n+1}\Delta\theta_{b2} + \Delta S_2\theta_{b1}^n + \Delta S_1\theta_{b2}^n\right) + \Delta M_{b2} = 0 \tag{46}$$

Depending on the state of the spring elements, $\Delta\theta_{bi}$ has different expressions. Specifically, when the spring element at both ends of the element is in either an elastic or elastoplastic state, the formulas for $\Delta\theta_{bi}$ are shown below,

$$\Delta\theta_{b1} = \left(\left(S_1^{n+1} + S_{s2}^n\right)\left(S_{s1}^n\Delta\theta_{s1} - \Delta S_1\theta_{b1}^n - \Delta S_2\theta_{b2}^n\right) - S_2^{n+1}\left(S_{s2}^n\Delta\theta_{s2} - \Delta S_2\theta_{b1}^n - \Delta S_1\theta_{b2}^n\right)\right)/\beta_1 \tag{47}$$

$$\Delta\theta_{b2} = \left(\left(S_1^{n+1} + S_{s1}^n\right)\left(S_{s2}^n\Delta\theta_{s2} - \Delta S_2\theta_{b1}^n - \Delta S_1\theta_{b2}^n\right) - S_2^{n+1}\left(S_{s1}^n\Delta\theta_{s1} - \Delta S_1\theta_{b1}^n - \Delta S_2\theta_{b2}^n\right)\right)/\beta_1 \tag{48}$$

and

$$\beta_1 = \left(S_1^{n+1} + S_{s1}^n\right)\left(S_1^{n+1} + S_{s2}^n\right) - \left(S_2^{n+1}\right)^2 \tag{49}$$

If a fully plastic hinge is formed at node 1 of the element,

$$\Delta\theta_{b1} = \left(\left(S_1^{n+1} + S_{s2}^n\right)\left(\Delta M_{pr,1} - \Delta S_1\theta_{b1}^n - \Delta S_2\theta_{b2}^n\right) - S_2^{n+1}\left(S_{s2}^n\Delta\theta_{s2} - \Delta S_2\theta_{b1}^n - \Delta S_1\theta_{b2}^n\right)\right)/\beta_2 \tag{50}$$

$$\Delta\theta_{b2} = \left(\left(S_1^{n+1} + S_{s1}^n\right)\left(S_{s2}^n\Delta\theta_{s2} - \Delta S_2\theta_{b1}^n - \Delta S_1\theta_{b2}^n\right) - S_2^{n+1}\left(\Delta M_{pr,1} - \Delta S_1\theta_{b1}^n - \Delta S_2\theta_{b2}^n\right)\right)/\beta_2 \tag{51}$$

and

$$\beta_2 = S_1^{n+1}\left(S_1^{n+1} + S_{s2}^n\right) - \left(S_2^{n+1}\right)^2 \tag{52}$$

If a fully plastic hinge is formed at node 2 of the element,

$$\Delta\theta_{b1} = \left(S_1^{n+1}\left(S_{s1}^n\Delta\theta_{s1} - \Delta S_1\theta_{b1}^n - \Delta S_2\theta_{b2}^n\right) - S_2^{n+1}\left(\Delta M_{pr,2} - \Delta S_2\theta_{b1}^n - \Delta S_1\theta_{b2}^n\right)\right)/\beta_3 \tag{53}$$

$$\Delta\theta_{b2} = \left(\left(S_1^{n+1} + S_{s1}^n\right)\left(\Delta M_{pr,2} - \Delta S_2\theta_{b1}^n - \Delta S_1\theta_{b2}^n\right) - S_2^{n+1}\left(S_{s1}^n\Delta\theta_{s1} - \Delta S_1\theta_{b1}^n - \Delta S_2\theta_{b2}^n\right)\right)/\beta_3 \tag{54}$$

and

$$\beta_3 = S_1^{n+1}\left(S_1^{n+1} + S_{s1}^n\right) - \left(S_2^{n+1}\right)^2 \tag{55}$$

When the element forms fully plastic hinges at both ends,

$$\Delta\theta_{b1} = \left(S_1^{n+1}\left(\Delta M_{pr} - \Delta S_1\theta_{b1}^n - \Delta S_2\theta_{b2}^n\right) - S_2^{n+1}\left(\Delta M_{pr} - \Delta S_2\theta_{b1}^n - \Delta S_1\theta_{b2}^n\right)\right)/\beta_4 \tag{56}$$

$$\Delta\theta_{b2} = \left(S_1^{n+1}\left(\Delta M_{pr} - \Delta S_2\theta_{b1}^n - \Delta S_1\theta_{b2}^n\right) - S_2^{n+1}\left(\Delta M_{pr} - \Delta S_1\theta_{b1}^n - \Delta S_2\theta_{b2}^n\right)\right)/\beta_4 \tag{57}$$

and

$$\beta_4 = \left(S_1^{n+1}\right)^2 - \left(S_2^{n+1}\right)^2 \tag{58}$$

Once $\Delta\theta_{bi}$ is computed, the incremental forces of the integrated element can be obtained readily through Eqs. (35-42). Subsequently, the internal forces of the element for the current load step are updated. The co-rotational method is then applied to transform these forces into the global coordinate system. Finally, these forces are assembled to achieve force recovery for the entire structure.

5. Numerical examples

The present study adopts the load control Newton-Raphson method to conduct the second-order inelastic analysis of steel frame structures. In this section, the accuracy and efficacy of the proposed methodology are verified through several benchmark problems. The results from the BEAM188 element within the commercial software ANSYS, utilizing the plastic zone model, serve as the benchmark for precise solutions in these numerical examples. It is noted that the spring sections at both ends of the beam-column elements need to be discretized before the calculation begins. For all present examples, the wide flange section features a precise division into 16 layers, with uniform thickness across the 8 layers for each web and the 4 layers allocated for the flange.

5.1. Cantilever beam under vertical end point load

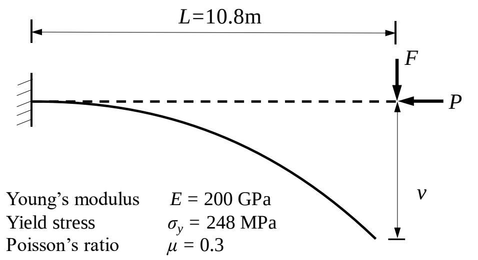

Fig. 13. Cantilever beam under vertical end point load

The cantilever beam depicted in Fig. 13 is subjected to the combined action of shear and axial forces at its free end. The cantilever beam, constructed from a wide flange section of W21×50, measures 10.8 meters in length. The Young's modulus E and yield stress σ_y of the material are 200 GPa and 248 MPa, respectively. The Poisson's ratio μ is 0.3. The shear force F is defined as M_p/L, and the axial forces are taken as 0, $0.2P_y$, $0.4P_y$, and $0.6P_y$, respectively. In this example, the cantilever member is simulated by only one proposed integrated element, and the applied loads are increased proportionally until the cantilever beam fails. Fig. 14 compares the vertical displacements at the free end of the cantilever beam, as determined by this study, with the results obtained from a simulation using 100 BEAM188 elements in ANSYS.

It can be seen from Fig. 14 that the results given by the present study and the BEAM188 element in ANSYS have good agreement. The present second-order inelastic analysis of steel frame structures only needs one proposed element to achieve accurate results in this example. Therefore, the present improved fiber plastic hinge model matches the accuracy of the plastic zone model, yet it offers superior efficiency in computational performance.

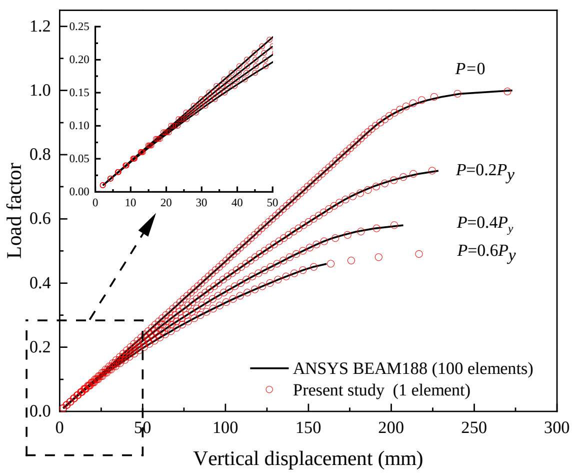

Fig. 14. Load-displacement curve of cantilever beam

5.2. Fixed-end Beam

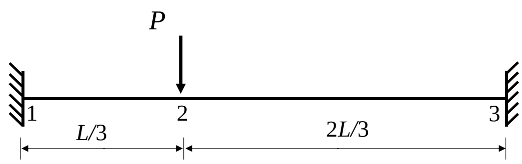

Fig. 15. Fixed-end beam subjected to shear force at $L/3$

Fig. 15 shows a beam with fixed supports at both ends and subjected to a vertical force P=8000 kN at one-third the distance from the left support. This example was first investigated by Liew et al. [27] to verify their proposed refined plastic hinge method. The beam measures 6 meters in length and features a W8×48 cross-sectional profile. The Young's modulus E and yield stress σ_y of the material are 205 GPa and 235 MPa, respectively. In the present analysis, the beam is simulated by two proposed elements, with the loading point coinciding with a node. For comparative analysis, this benchmark problem was also examined using a mesh of 100 BEAM188 elements within the ANSYS software. In both analytical approaches, the vertical point force P is incrementally applied until the analysis fails to converge.

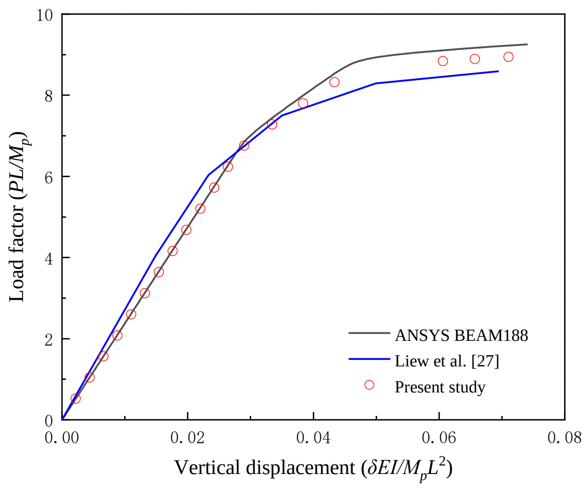

Fig. 16. Bending load-displacement curve of a major axis of fixed-end beam

Fig. 16 illustrates a comparative analysis of vertical displacements δ at the load application point, showcasing results from the current study, simulations using BEAM188 elements in ANSYS, and the refined plastic hinge method proposed by Liew et al. [27]. It can be seen that the present results are very close to those of 100 BEAM188 elements in ANSYS with only two elements in this example. Moreover, the accuracy of the proposed improved fiber plastic hinge method surpasses that of the conventional plastic hinge method, as it achieves a level of precision comparable to the plastic zone method.

5.3. Single-layer Portal Frame

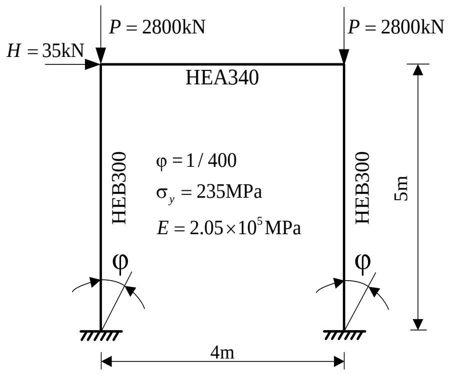

Fig. 17. Single-layer portal frame

Fig. 17 illustrates a single-layer portal frame, a classic structural problem initially introduced by Vogel et al. [28] in 1985. Many researchers have used this example to verify their analysis methods for steel frame structures. The portal frame comprises two 5-meter-high columns, each featuring a HEB300 cross-section, and a 4-meter-long beam with a HEA340 cross-section. The single-layer portal frame is rigidly fixed at its base, with both columns exhibiting an initial inclination angle of φ=1/400 relative to the column height. The yield stress for all members of the portal frame σ_y is 235 MPa, and the Young's modulus E is 205 GPa. A horizontal force H=35 kN and two vertical forces P=2800 kN are applied on the top of the frame. Consequently, the frame is expected to experience sway, and the columns will exhibit second-order effects under these loads.

In this example, the portal frame is modeled by one proposed element per member, and the loads are applied proportionally in the analysis until the frame reaches its failure point. Fig. 18 displays the lateral displacement outcomes for the left top of the frame, compared with those given by the BEAM188 element in ANSYS and the traditional plastic hinge method proposed by Vogel et al. [28]. In the ANSYS simulation, each member of the portal frame is modeled using 100 BEAM188 elements, which allows the obtained solutions to be considered precise. It can be seen from Fig. 18 that the results given by the present study and the BEAM188 element are very close to each other, therefore the proposed improved fiber plastic hinge method is more accurate than the traditional plastic hinge method and has the same precise as the plastic zone method. Furthermore, the present study can achieve accurate results with a simulation employing just one element per member, offering significantly greater efficiency than the plastic zone method.

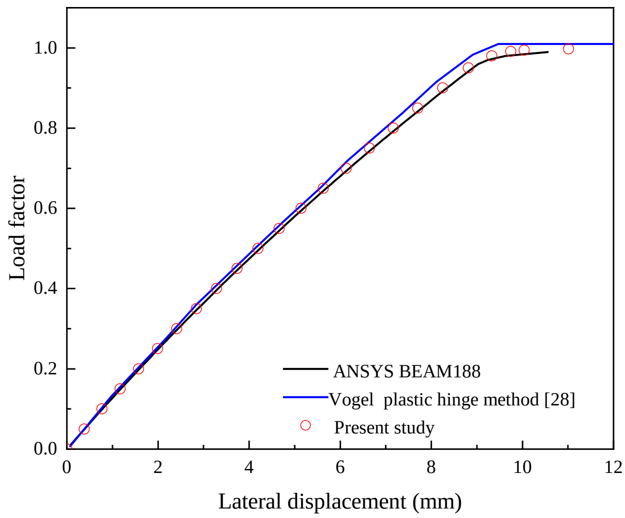

Fig. 18. Load-displacement curve of single-layer portal frame

5.4. Two-span four-layer frame

Fig. 19 shows a two-span four-story frame which was investigated by Yang et al. [29] to verify their present elastoplastic analysis of steel frames based on the traditional plastic hinge method. The geometry, boundary conditions, and loading of the frame are depicted in Fig. 19. In this analysis, each column was simulated by a single proposed beam-column element, while each beam was modeled using two proposed elements, with the loading point coinciding with the node. The present research employs the Newton-Raphson method for the incremental-iterative analysis of this example, gradually increasing the applied loads in proportion until the steel frame reaches its failure threshold. Fig. 20 plots the lateral displacements (Δ) of the frame from the present study, alongside a comparison with the outcomes from the BEAM188 element in ANSYS and the analytical approach suggested by Yang et al. [29]. Specifically, each beam and column of the frame are simulated by 20 BEAM188 elements in ANSYS, employing the Newton-Raphson method to iterate until the frame experiences failure. The analysis method proposed by Yang et al. [29] which is based on the traditional plastic hinge method, adopted the same mesh of the frame as the present study. However, it utilized the generalized displacement control method which can get the solutions after the structural failure occurs.

Through the comparison presented in Fig. 20, it is evident that the proposed analysis method based on the improved fiber plastic hinge approach, exhibits a strikingly similar level of accuracy compared to the simulations conducted using 20 BEAM188 elements per member in ANSYS. Also, the difference between the traditional plastic hinge method [29] and the plastic zone method (the BEAM188 element in ANSYS) is obvious in this example. The proposed plastic hinge method improved by the discretization of the hinge section, offers a high degree of precision that closely matches the plastic zone method, and provides greater efficiency.

6. Conclusions

This paper introduces an innovative plastic hinge method, termed the "improved fiber plastic hinge method," which is predicated on the discretization of the hinge section, offering a refined approach to structural analysis. The improved fiber plastic hinge method is capable of accurately calculating the ultimate elastic and plastic moment capacities, as well as the moment-curvature relationship. Thus, it is more accurate than the traditional plastic hinge method which commonly depends on an empirical and simplified formula.

The present second-order inelastic analysis of steel frame structures, which employs the improved fiber plastic hinge method, has been rigorously validated through several benchmark numerical examples. The present results for these examples were compared with the plastic zone method which is the BEAM188 element in ANSYS and conventional plastic hinge methods. The findings indicate that the accuracy of the present study not only outperforms conventional plastic hinge methodologies but also achieves a comparable level of accuracy to the plastic zone method. However, the present study is more efficient than the plastic zone method, as it requires merely one or two elements per member to achieve precise outcomes. Moreover, the improved fiber plastic hinge method holds significant promise over traditional approaches, as it is capable of accurately accounting for the impacts of residual and transverse shear stresses. These aspects are slated for exploration in our forthcoming research endeavors.

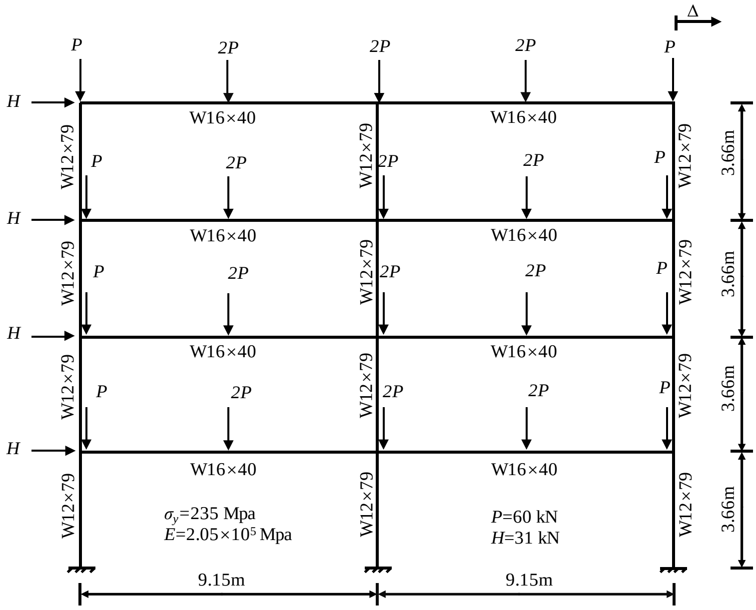

Fig. 19. Two-span four-story frame structure and calculation information

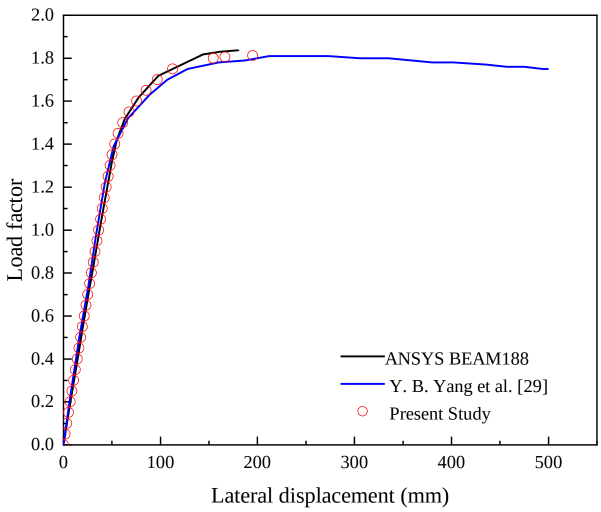

Fig. 20. Load-displacement curve of two-span four-story frame

Acknowledgments

The research described in this paper was financially supported by the National Natural Science Foundation of China (52108120), the Natural Science Foundation of Jiangsu Province (BK20210258), and the Fundamental Research Funds for the Central Universities (2242024k30065).

References

[1] Trahair, N. S., "Trends in the code design of steel framed structures", Advanced Steel Construction, WOS, 2018, 14(1): 37–56.

[2] Kim, S. E., Park, M. H. and Choi, S. H., "Direct design of three-dimensional frames using practical advanced analysis", Engineering Structures, Elsevier, 2001, 23(11): 1491-1502.

[3] Iu, C. K. and Bradford, M. A., "Higher-order non-linear analysis of steel structures. Part II: Refined Plastic Hinge Formulation", Advanced Steel Construction, WOS, 2011, 8(2): 183-198.

[4] Iu, C. K. and Bradford, M. A., "Higher-order non-linear analysis of steel structures. Part I: Elastic Second-Order Formulation", Advanced Steel Construction, WOS, 2011, 8(2): 168-183.

[5] Zhou, Z. H. and Chan, S. L., "Elastoplastic and large deflection analysis of steel frames by one element per member. I: One Hinge along Member", Journal of Structural Engineering, ASCE, 2004, 130(4): 538-544.

[6] Zhou, Z. H. and Chan, S. L., "Elastoplastic and large deflection analysis of steel frames by one element per member. II: Three Hinges along Member", Journal of Structural Engineering, ASCE, 2004, 130(4): 545-553.

[7] Wen, R. K. and Lange, J., "Curved beam element for arch buckling analysis", Journal of the Structural Division, ASCE, 1981, 107(11): 2053-2069.

[8] Van, L. H. and Dang, H. N., "Second-order plastic-hinge analysis of 3-D steel frames including strain hardening effects", Engineering Structures, Elsevier, 2008, 30(12): 3505-3512.

[9] Thai, H. T. and Kim, S. E., "Second-order inelastic dynamic analysis of steel frames using fiber hinge method", Journal of Constructional Steel Research, Elsevier, 2011, 67(10): 1485-1494.

[10] Lu, C. K. and Bradford, M. A., "Second-order elastic finite element analysis of steel structures using a single element per member", Engineering Structures, Elsevier, 2010, 32(9): 2606–2616.

[11] Chan, S. L. and Zhou, Z. H., "Pointwise equilibrating polynomial element for nonlinear analysis of frames", Journal of Structural Engineering, ASCE, 1994, 120(6): 1703–1717.

[12] Chan, S. L. and Zhou, Z. H., "Second-order elastic analysis of frames using single imperfect element per member", Journal of Structural Engineering, ASCE, 1995,121(6): 939–945.

[13] Tang, Y. Q., Liu, Y. P. and Chan, S. L., "An innovative co-rotational pointwise equilibrating polynomial element based on Timoshenko beam theory for second-order analysis", Thin-Walled Structures, Elsevier, 2019, 141: 15-27.

[14] Doan-Ngoc, T. N., Dang, X. L. and Ngo-Huu, C., "Second-order plastic-hinge analysis of planar steel frames using corotational beam-column element", Journal of Constructional Steel Research, Elsevier, 2016, 121: 413–426.

[15] Kassimali, A., "Large deformation analysis of elastic-plastic frames", Journal of Structural Engineering, ASCE, 1983, 109(8): 1869–1886.

[16] Liew, J. Y. R., White, D. W. and Chen, W. F., "Second-order refined-plastic hinge analysis for frame design. Part I", Journal of Structural Engineering, ASCE, 1993, 119 (11): 3196–3216.

[17] Nguyen, P. C. and Kim, S. E., "Nonlinear inelastic time-history analysis of three-dimensional semi-rigid steel frames", Journal of Constructional Steel Research, Elsevier, 2014, 101: 192-206.

[18] Zhou, Y., Hu, B., Gong, Y., Tang, L. and Li, Y., "Second-order improved refined plastic hinge method with implementation of continuous strength method", Journal of Constructional Steel Research, [19] Elsevier, 2023, 211: 108169.

[19] Liu, S. W., Liu, Y. P. and Chan, S. L., "Direct analysis by an arbitrarily-located-plastic-hinge element - part 1: planar analysis", Journal of Constructional Steel Research, Elsevier, 2014, 103: 303–315.

[20] Liu, S. W., Liu, Y. P. and Chan, S. L., "Direct analysis by an arbitrarily-located-plastic-hinge element - part 2: spatial analysis", Journal of Constructional Steel Research, Elsevier, 2014, 103: 316–326.

[21] Fieber, A., Gardner, L. and Macorini, L., "Structural steel design using second-order inelastic analysis with strain limits", Journal of Constructional Steel Research, Elsevier, 2020, 168: 105980.

[22] Fieber, A., Gardner, L. and Macorini, L., "Design of structural steel members by advanced inelastic analysis with strain limits", Engineering Structures, Elsevier, 2019, 199: 109624.

[23] Gardner, L., Yun, X., Fieber, A. and Macorini, L., "Steel design by advanced analysis: material modeling and strain limits", Engineering, Elsevier, 2019, 5 (2): 243–249.

[24] Walport, F., Gardner, L. and Nethercot, D. A., "Design of structural stainless steel members by second order inelastic analysis with CSM strain limits", Thin-Walled Structures, Elsevier, 2020, 159: 107267.

[25] Quan, C. Y., Kucukler, M. and Gardner, L., "Design of web-tapered steel I-section members by second-order inelastic analysis with strain limits", Engineering Structures, Elsevier, 2020, 224: 111242.

[26] Tang, Y. Q., Zhu, H. and Du, E F., "A novel incremental iterative force recovery method for second-order beam-column elements in plastic hinge analysis of steel frames", International Journal of Structural Stability and Dynamics, WOS, 2022, 22(02): 2250027.

[27] Liew, J. Y. R., White, D. W., Chen, W. F., "Second-order refined plastic hinge analysis of Frames", Journal of Structural Engineering, ASCE, 1992, 119:11.

[28] Vogel, U., "Calibrating frames", Stahlbau, 1986, 10(55): 295-301.

[29] Yang, Y. B., Chen, Z. H. and Tao, Y. C., "Elastoplastic analysis of steel framed structures based on rigid body rule and plastic-hinge concept", International Journal of Structural Stability and Dynamics, WOS, 2019, 19(09): 1950104.